

Article

Anionic Dye Removal Using a Date Palm Seed-Derived Activated Carbon/Chitosan Polymer Microbead Biocomposite

Hani Hussain Sait ^{1,*}, Ahmed Hussain ¹, Mohamed Bassyouni ^{2,3,*} , Imtiaz Ali ² , Ramesh Kanthasamy ², Bamidele Victor Ayodele ⁴ and Yasser Elhenawy ⁵ 

¹ Department of Mechanical Engineering, Faculty of Engineering Rabigh, King Abdulaziz University, Rabigh 21911, Saudi Arabia; ahmad@neduet.edu.pk

² Department of Chemical and Materials Engineering, Faculty of Engineering Rabigh, King Abdulaziz University, Rabigh 21911, Saudi Arabia; inabi@kau.edu.sa (I.A.); rsampo@kau.edu.sa (R.K.)

³ Department of Chemical Engineering, Faculty of Engineering, Port Said University, Port Fouad 42526, Egypt

⁴ Department of Chemical Engineering, Universiti Teknologi PETRONAS, Seri Iskandar 32610, Malaysia; ayodelebv@gmail.com

⁵ Department of Mechanical and Power Engineering, Faculty of Engineering, Port Said University, Port Fouad 42526, Egypt; dr_yasser@eng.psu.edu.eg

* Correspondence: hhsait@kau.edu.sa (H.H.S.); migb2000@gmail.com (M.B.)

Abstract: The discharge of textile wastewater into aquatic streams is considered a major challenge due to its effect on the water ecosystem. Direct blue 78 (DB78) dye has a complex structure. Therefore, it is difficult to separate it from industrial wastewater. In this study, carbon obtained from the pyrolysis of mixed palm seeds under different temperatures (400 °C and 1000 °C) was activated by a thermochemical method by using microwave radiation and an HCl solution in order to improve its adsorption characteristics. The generated activated carbon was used to synthesize a novel activated carbon/chitosan microbead (ACMB) for dye removal from textile wastewater. The obtained activated carbon (AC) was characterized by a physicochemical analysis that included, namely, particle size, zeta potential, SEM, EDX, and FTIR analyses. A series of batch experiments were conducted in terms of the ACMB dose, contact time, pH, and activated carbon/chitosan ratios in synthetic microbeads for enhancing the adsorption capacity. A remarkable improvement in the surface roughness was observed using SEM analysis. The particle surface was transformed from a slick surface with a minor-pore structure to a rough surface with major-pore structure. The zeta potential analysis indicated a higher improvement in the carbon surface charge, from −35 mv (before activation) to +20 mv (after activation). The adsorption tests showed that the dye-removal efficiency increased with the increasing adsorbent concentration. The maximum removal efficiencies were 97.8% and 98.4% using 3 and 4 g/L of AC_{400°C} MB-0.3:1 and AC_{1000°C} MB-0.3:1, respectively, with initial dye concentrations of 40 mg/L under acidic conditions (pH = 4–5), and an optimal mixing time of 50 min. The equilibrium studies for AC_{400°C} MB-0.3:1 and AC_{1000°C} MB-0.3:1 showed that the equilibrium data best fitted to the Langmuir isothermal model with R² = 0.99. These results reveal that activated carbon/chitosan microbeads are an effective adsorbent for the removal of direct blue 78 dye and provide a new platform for dye removal.

Keywords: activated carbon; microwave radiation; chitosan; microbeads; adsorption; isothermal models; direct dye removal



Citation: Sait, H.H.; Hussain, A.; Bassyouni, M.; Ali, I.; Kanthasamy, R.; Ayodele, B.V.; Elhenawy, Y. Anionic Dye Removal Using a Date Palm Seed-Derived Activated Carbon/Chitosan Polymer Microbead Biocomposite. *Polymers* **2022**, *14*, 2503. <https://doi.org/10.3390/polym14122503>

Academic Editor: Luminita Marin

Received: 2 May 2022

Accepted: 14 June 2022

Published: 20 June 2022

Publisher's Note: MDPI stays neutral with regard to jurisdictional claims in published maps and institutional affiliations.



Copyright: © 2022 by the authors. Licensee MDPI, Basel, Switzerland. This article is an open access article distributed under the terms and conditions of the Creative Commons Attribution (CC BY) license (<https://creativecommons.org/licenses/by/4.0/>).

1. Introduction

Water is considered the most effective and central substance in human life. Due to its major applications in various industries, water is exposed to several pollutants and can therefore be contaminated. In recent years, water pollution has become a major threat to water ecology, and thus the extraction of pollutants from industrial wastewater before discharging into water streams is essential [1]. Industrial wastewater mostly contains organic

and nonorganic contaminants that can be toxic to humans and aquatic life [2]. Amongst several pollutants, synthetic dyes are considered highly toxic and cancerogenic materials because they have complex aromatic structures that lead to difficult decomposition and separation [3]. Several industries, such as cosmetics, paper, textiles, printing, and pharmaceuticals, discharge large amounts of wastewater, which contain dyes and other toxic chemicals [4]. It was reported that 50×10^3 tons of organic dyes are disposed worldwide every year [5]. Synthetic dyes are classified into three categories: anionic (direct, acidic, and reactive), cationic (all base dyes), and nonanionic (dispersed dyes) [6,7]. It is stated that direct dye has a highly harmful effect on the environment because it has a high water solubility, which makes it extremely difficult to extract using traditional methods [8]. One of its characteristics is the capacity to spread color to a given substrate due to its molecular structure, which contains chromophoric groups. These colors disrupt the water bodies aesthetically, contributing to a decline in the rate of photosynthesis and dissolved oxygen levels, and affecting the entire aquatic biota [9].

Several methods have been investigated for dye removal from industrial wastewater, such as nanofiltration, ozonation, flocculation, adsorption, reverse osmosis, chemical oxidation, and electrochemical, biological, and photocatalytic degradation [10–15]. However, these treatment technologies have shown a number of limitations and disadvantages, including a lower validation of the removal of different pollutants, high costs, high reagent requirements, and the generation of toxic waste products, which require further safe disposal [8]. From these techniques, adsorption is considered the most versatile method, and it has received a lot of attention due to its advantages, such as flexibility, low-sludge production, low cost, efficiency, and high speed [16,17]. Many adsorbents have been used efficiently for dye removal from industrial wastewater, such as activated carbon, chitosan, fly ash, and zeolites [18–20].

Activated carbon (AC) has been investigated and used as a potential adsorbent in several processes, such as the treatment of industrial effluents [21], groundwater treatment [22], and dye removal [23]. AC confirms the major adsorption in the gas and liquid phases due to its high micropore volume (V_{mic}), large specific surface area (S_{BET}), favorable pore size distribution, thermal stability, capability of high-speed adsorption, and low acid/base reactivity [24]. The high cost of the AC production process is the most significant challenge for commercial manufacturers, and the use of inexpensive raw materials with high carbon contents and low levels of inorganic compounds to produce low-cost AC has been a focus of research efforts in recent years. Agricultural byproducts and waste materials, such as rice husks [25], coconut husks [26], and oil palm fibers [27], are among the low-cost precursors for the production of AC. Moreover, chitosan has been investigated for various applications due to its biocompatibility, biodegradability, and derivability from abundant and inexpensive biomass [28]. Chitosan and chitosan-based composite materials have been used as sorption materials with high efficiency [29]. Chitosan hydrogel beads were produced by lowering the degree of crystallinity by generating a gel with the purpose of raising chitosan's adsorption capability. Several strategies, including chemical crosslinking with cross-linking agents on their surface, have been developed to improve the commercial applicability of chitosan beads as an adsorbent material [30].

This study aims to develop a novel microbead composite adsorbent from activated carbon (AC) and chitosan hydrogel. AC was generated from the pyrolysis of mixed date palm seeds (DPS) under temperatures of 400 °C and 1000 °C, followed by the activation process using microwave radiation. These novel microbeads were used efficiently as an adsorbent material for the direct blue 78 (DB78)-dye-removal process.

2. Materials and Methods

2.1. Preparation of Activated Carbon (AC)

Two carbon samples, obtained from the pyrolysis of mixed date palm seeds (DPS) under temperatures of 400 °C and 1000 °C, were used in this study [31]. The carbon samples were placed into 400 mL distilled water. The solution was stirred 4 h with a mixing speed

of 200 RPM at 30 °C. Samples were washed, filtered using a Whatman filter paper, and left to dry at 110 °C for 12 h using a thermal dryer. In order to activate the carbon, the samples were subjected to a microwave-chemical-activation process. These samples were activated by immersing 15 g of carbon into 250 mL of an HCl solution, with a concentration of 7% wt/wt, and then the solution was placed into a domestic microwave (frequency: 2.45 GHz; power: 600 W) for a contact time of 6 min. At the end of the activation process, the mixture was filtrated using a Whatman filter paper, washed using distilled water, and left to dry at 110 °C for 24 h. Physical and chemical analyses were conducted to characterize the activated carbon.

2.2. Chitosan and Dye

Chitosan is an amino-based polymer that is synthesized in vast amounts by the N-deacetylation of chitin. The characteristics of the chitosan used in this study are a white powder with a molecular weight range from 140 to 220 kDa, a degree of deacetylation (DAC) = 81.2%, viscosity = 36,000 cps, and a density of 0.15 g/mL. The chemical structure of chitosan is shown in Figure 1a.

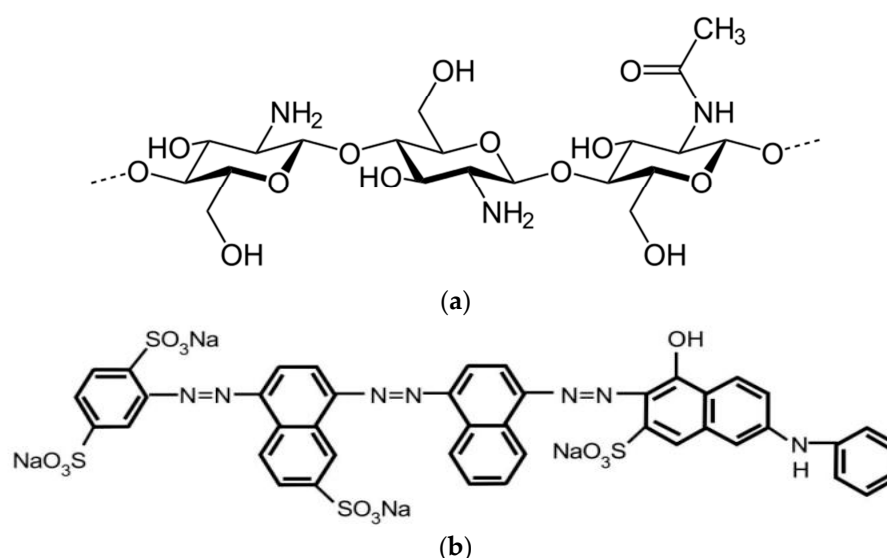


Figure 1. The chemical structure of (a) chitosan and (b) DB78 dye.

The direct blue 78 (DB78) dye had a relative molecular mass of 1059.95, a maximum wavelength of $\lambda_{\max} = 604$ nm, and solubility up to 10 g/L at 25 °C. The direct blue 78 was selected for adsorption tests as it is widely used in the textile industry. The chemical structure of direct blue 78 is shown in Figure 1b.

2.3. Preparation of Activated Carbon/Chitosan Microbeads (ACMB)

Activated carbon/chitosan microbeads (ACMB) with different ratios of activated carbon to chitosan were synthesized. In AC_mMB-z, m and z refer to the pyrolysis temperatures for carbon extraction (400 °C and 1000 °C) and the ratio of AC to chitosan, respectively. The adsorption studies were conducted using polymer-based composite materials with different mixing ratios: AC_mMB-0.1:1, AC_mMB-0.2:1, AC_mMB-0.3:1, AC_mMB-0.4:1, and AC_mMB-0.5:1. In AC_{400°C} MB-0.3:1, the chitosan solution was prepared under magnetic stirring for 3 h by dissolving 1.5 g (1.5 wt.%) of chitosan powder in diluted acetic acid to form 100 mL of chitosan hydrogel. A total of 450 mg from activated carbon (pyrolysis temperature: 400 °C), representing 0.45 wt.%, was added to the formed hydrogel (45 mg of AC was added to 10 mL of chitosan hydrogel under magnetic stirring for 4 h and a temperature of 60 °C). The final prepared gel was dropped into a 0.7 M NaOH solution (contact time: 3 h) using a micropipette to form the beads. The formed beads were then

washed using distilled water. Finally, the beads were oven-dried at 60 °C. The preparation process is illustrated in Figure 2.

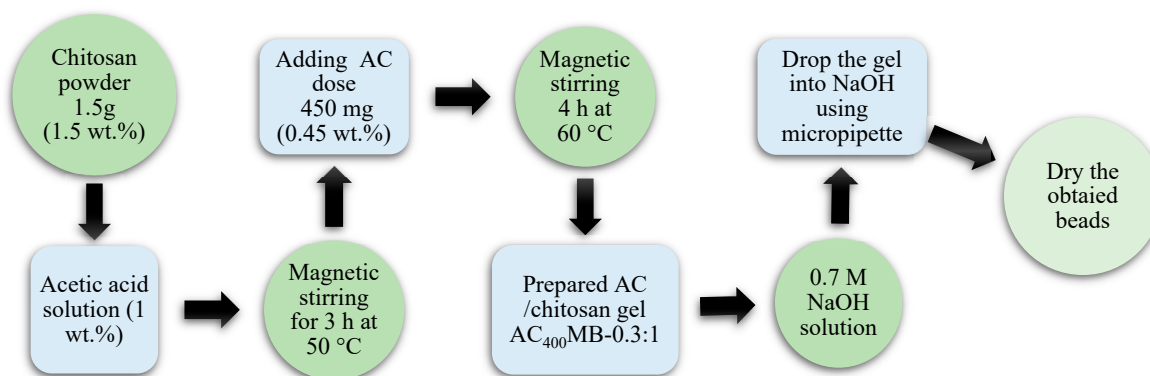


Figure 2. The preparation process for activated carbon/chitosan beads (AC_{400°C} MB-0.3:1).

2.4. Adsorption Studies

This study was conducted using the batch adsorption system (lab scale) on single-component synthetic wastewater. The activated carbon/chitosan microbead dose used in this study was 0.5–6.5 g. Synthetic wastewater with an initial concentration of 40 mg/L was mixed with ACMB at 200 RPM for the contact time (0–100) minimum at room temperature (25 ± 2 °C). The spectrophotometrically analysis was applied to determine the removal efficiency by measuring the dye concentration before and after the adsorption process at $\lambda_{\max} = 600$ nm for DB78, as given in Equation (1):

$$\%(\text{R}) = \frac{C_0 - C}{C_0} \times 100 \quad (1)$$

Equilibrium loading can be determined by using Equation (2):

$$\text{Equilibrium loading, mg/g} = (C_0 - C) \times V/m \quad (2)$$

where C_0 and C are the initial and equilibrium concentrations of pollutant, respectively; V is the volume of solution (L); and m is the quantity of adsorbent (g).

2.5. Characterization of Materials

The activated carbon suspension was diluted in water and sonicated for 30 min in an ultrasonic bath at 4% (w/v). Model USC-1400 is one of a kind (40 kHz of ultrasound frequency). The Malvern 3000 Zetasizer NanoZS (Malvern Instruments, Malvern, UK) was used to measure the average particle size of produced activated carbon at 400 °C and 1000 °C. It measures the diffusion of particles moving under Brownian motion, and it translates the data to size and size distribution using dynamic light scattering. It is also used in laser doppler microelectrophoresis to provide an electric field to a dispersion of particles, which then move at a rate proportional to their zeta potential. The Smoluchowski algorithm was used to determine the particle size. Prior to adsorption studies, the samples were degasified at 200 °C for 4 h, and then the surface area was measured in the presence of N_2 adsorption at -195.65 °C using surface-area analyzers (Autosorb-I-C-8, Quantachrome, Boynton Beach, FL, USA). By applying the BET (Brunauer–Emmett–Teller) equation to the adsorption data, the BET surface area for the sample was determined.

FTIR studies for all samples were conducted using a VERTEX 80v vacuum FTIR Spectrometer, Bruker corporation, Germany. The surface morphology and porous microstructure of samples were investigated by SEM analysis (TESCAN MIRA-High Resolution scanning electron microscope, Tescan Essence company, Brno, Czech Republic).

Surface morphology and elemental analysis were performed using field-emission scanning electron microscopy (TESCAN MIRA-High Resolution scanning electron microscope,

Tescan Essence company, Brno, Czech Republic) coupled with an energy-dispersive X-ray (EDX) (Oxford instrument nano analysis detector, UK).

The colorimetric analysis was carried out in this study using a LAMOTTE smart spectrophotometer v3 2000-01-MN, Washington Ave. Chestertown, MD, USA.

3. Results and Discussion

3.1. Characterization of Adsorbents

The adsorbent samples were characterized by using a zeta sizer to measure the particle size. The zeta potential was used to measure the carbon particles' net surface charge, and BET analysis was conducted to determine the surface area. The surface morphology was investigated by using SEM analysis. The elemental analysis was studied by using EDX analysis. The chemical function groups were determined by using FTIR analysis.

3.1.1. Zeta Sizer Analysis

Due to its major effect and great influence on the adsorption process, the particle size distribution of activated carbon was investigated. Figure 3 shows that 96.5% of the AC₄₀₀ (activated carbon from a pyrolysis temperature of 400 °C) had average particle sizes less than 1.6 μm. For the AC_{1000°C} (activated carbon from a pyrolysis temperature of 1000 °C), 97.5% of the particle sizes were less than 1.2 μm. It was reported that there is an inverse relationship between the particle size and the adsorption capacity. The smaller the particle size, the higher the available surface area, which leads to a maximum adsorption capacity [32].

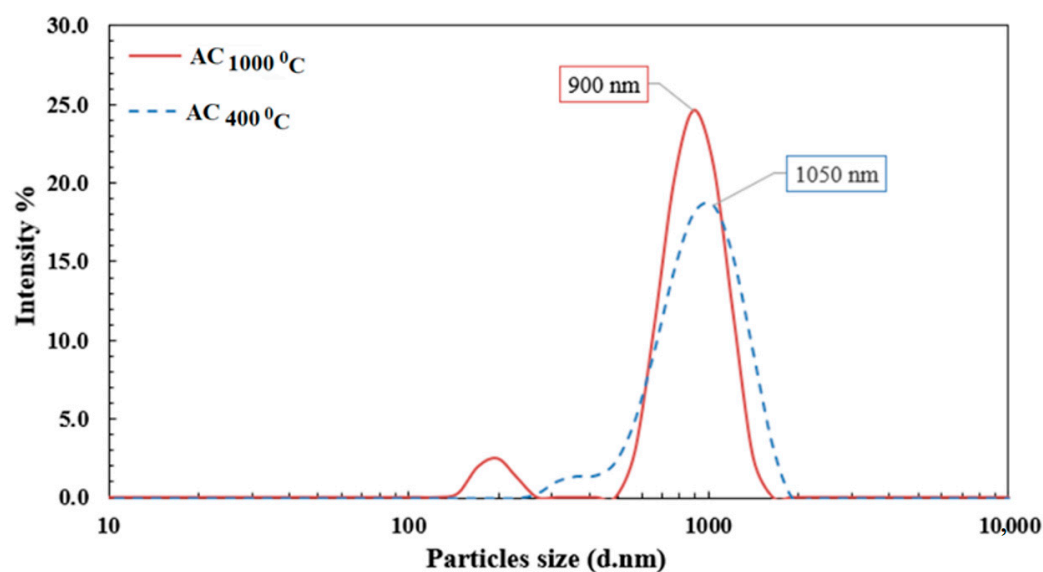


Figure 3. Particle-size-distribution analysis for activated carbon samples.

3.1.2. Zeta Potential Analysis

It was observed from the zeta potential analysis that the activation process using the HCl solution and microwave radiation has a remarkable effect on the surface charge of carbon particles. As illustrated in Figure 4a,b, carbon produced at high temperatures (1000 °C) has very hydrophobic behavior. However, due to the dehydration and deoxygenation of the palm seeds, it has reduced amounts of H- and O-containing functional groups. Surface groups can act as electron donors or acceptors, resulting in the creation of coexisting zones with a variety of characteristics that range from acidic to basic and from hydrophilic to hydrophobic. As a result, the ion-exchange capacity of carbon particles may be reduced. Biochar generated at lower temperatures (400 °C) has a more varied organic character due to the presence of aliphatic and cellulose-type structures. As a result, biochar's structure looks to have less surface-functional-group content as the temperature

increases. The surface charges of carbon particles were +5 mV and −35 mV, respectively, for carbon at 400 °C and 1000 °C. Figure 4a,b shows that the activation of carbon particles using acidic solution led to an increase in the positive charge to +30 mV and +20 mV for AC_{400°C} and AC_{1000°C}, respectively. This improvement in the surface charge is attributed to the accumulation of hydrogen ions (H⁺) on the activated carbon particle surface after the thermochemical modification process using microwave radiation and the HCl solution (chemical agent).

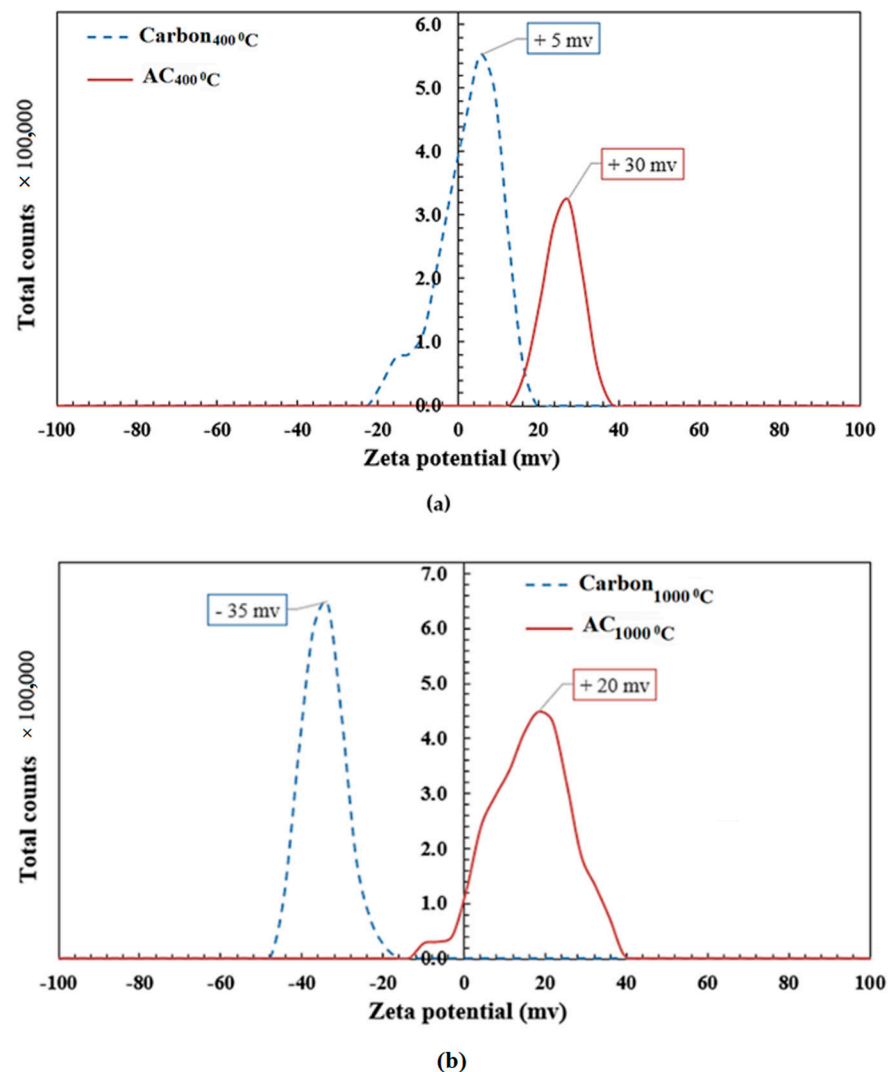


Figure 4. Effect of activation process on carbon surface charge of (a) carbon at 400 °C and (b) carbon at 1000 °C.

3.1.3. Energy-Dispersive X-ray (EDX) Analysis

In order to determine the carbon content and presence of different elements in the two types of activated carbon samples (AC_{400°C} and AC_{1000°C}), the energy-dispersive X-ray (EDX) analysis was conducted. Figure 5a shows peaks at ~0.2, 1.2, 2, and 3.5 KeV. These peaks are attributed to carbon (C), magnesium (Mg), phosphorus (P), and potassium (K), respectively. The elemental analysis for the AC_{400°C} sample indicated the presence of high carbon content (86.7%). For the AC_{1000°C}, peaks are observed at 0.2 and 3.5 KeV. These peaks are attributed to carbon (C) and potassium (K), respectively. Furthermore, the elemental analysis for the AC_{1000°C} sample indicated the presence of a higher carbon content (97.4%) than the carbon contents for the AC_{400°C}. These results are in good agreement with the reported data, as changes in the structure and physicochemical characteristics of biochar

are significantly associated with the pyrolysis temperature. The temperature of pyrolysis has a significant impact on the physicochemical characteristics of biochar (e.g., surface area, pH, and functional groups). The surface area, carbonized fractions, pH, and volatile matter increased as the pyrolysis temperature increased, whereas the cation-exchange capacity and content of the surface functional groups decreased.

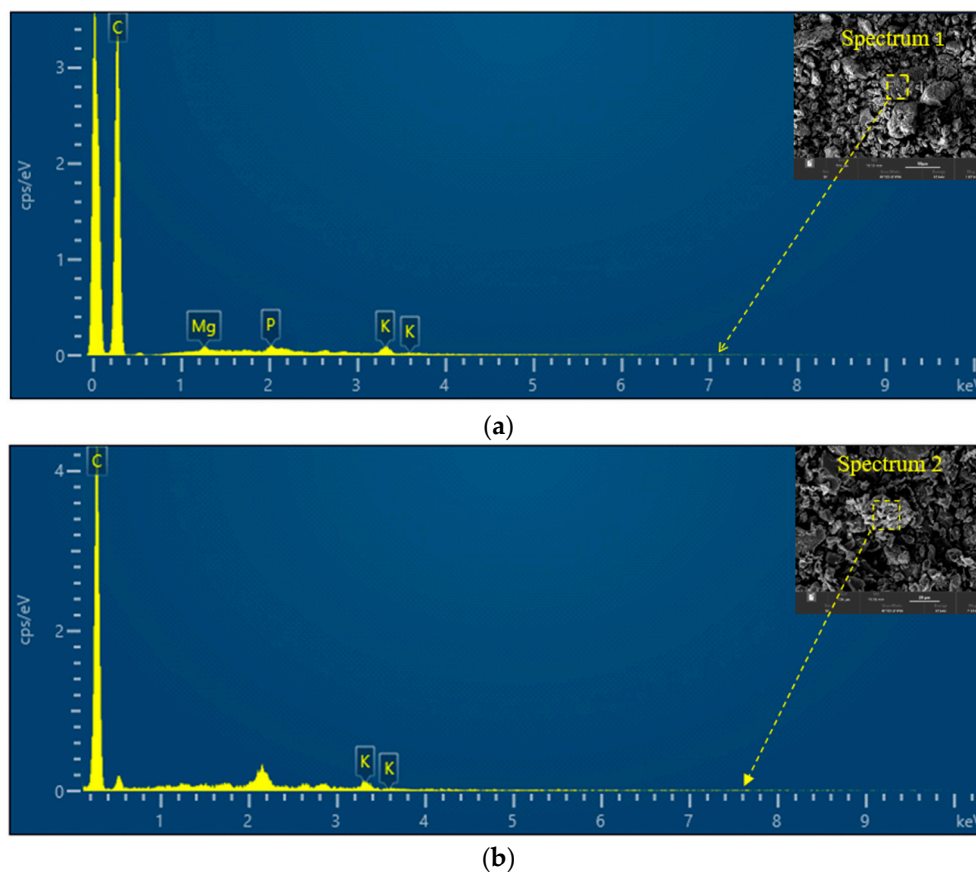


Figure 5. EDX analysis for charge: (a) activated carbon at 400 °C and (b) activated carbon at 1000 °C.

3.1.4. Scanning Electron Microscopy (SEM) Analysis

An SEM analysis was conducted to study the impact of the thermochemical activation process using the HCl solution and microwave radiation on the carbon surface morphology and the pore's structure. Figure 6a,c shows that the carbon obtained from the pyrolysis of date palm seeds (DPS) under temperatures of 400 °C and 1000 °C had a smooth and slick surface with a restricted pore structure. The two carbon samples had macropore diameters that ranged from 0.71–0.82 μm to 2.13:2.7 μm for carbon at 400 °C and 1000 °C, respectively. After the activation process, the carbon particles had a noticeable variation, as is shown in Figure 6b,d. The surface converted from a slick surface to an eroded rough surface, with a remarkable improvement in the porous structure. As a result of this major change in the surface morphology, the two activated carbon samples showed larger pore diameters. The pore size increased from 5.2 to 5.94 μm and from 3.70 to 4.71 μm at 400 °C and 1000 °C, respectively. This large improvement in the carbon physical characteristics can be attributed to the direct interaction between the microwave radiation and the particles inside the pressed compact material in the presence of HCl as a chemical agent. Figure 6e shows the distribution of the carbon particles (AC_{1000°C}) in the chitosan matrix. The activated carbon was found to be capable of dispersing effectively in chitosan, and forming composite beads with no agglomerations.

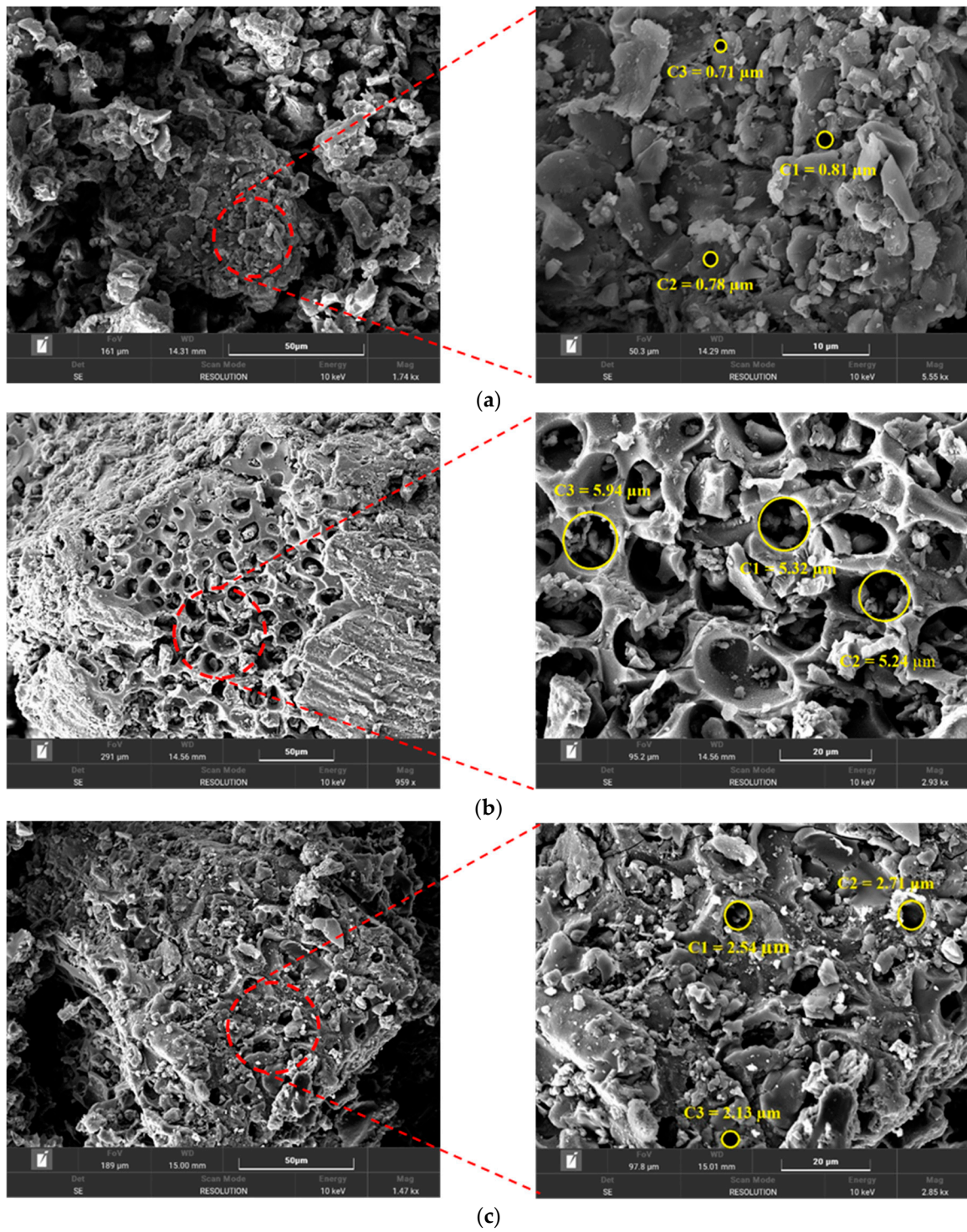


Figure 6. Cont.

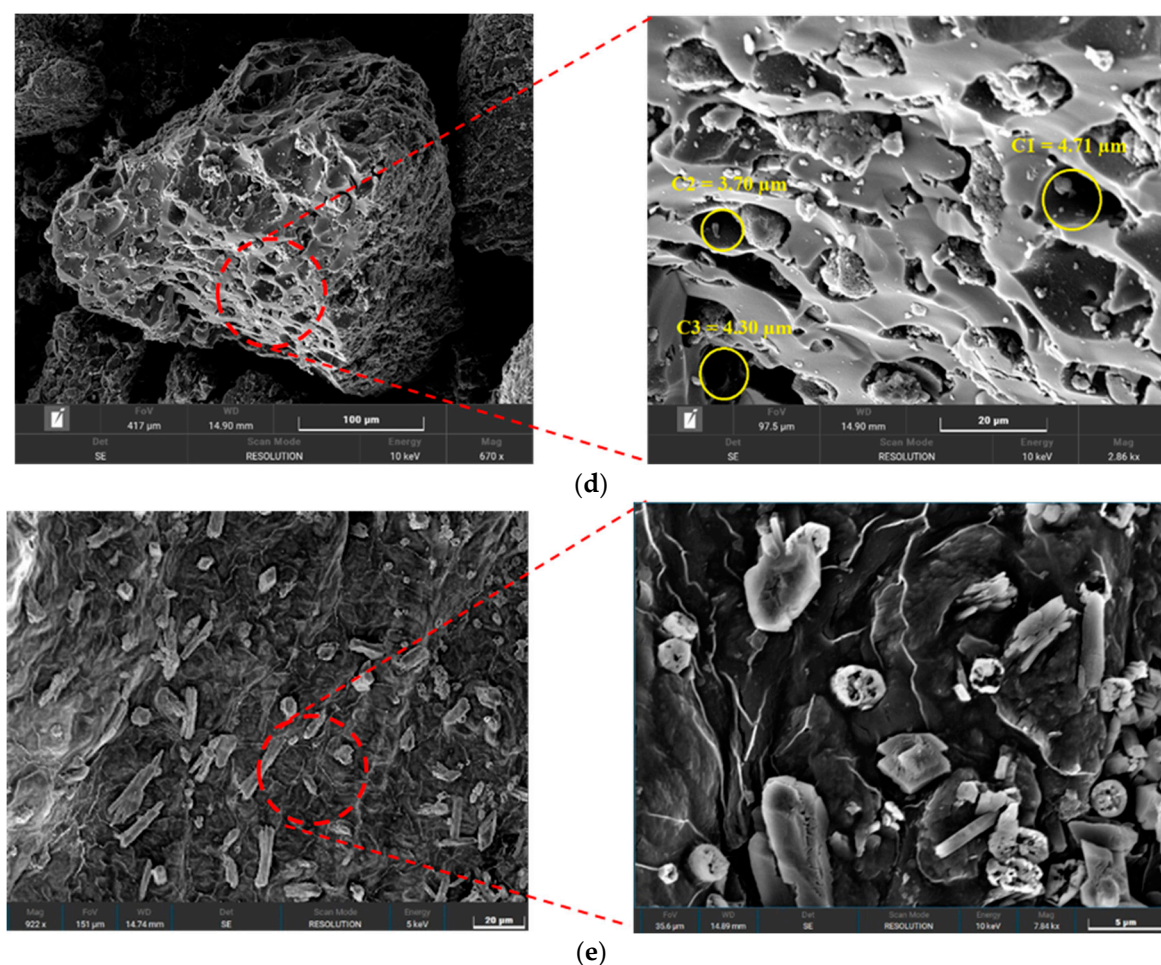


Figure 6. SEM analysis for (a) carbon at 400 °C, (b) activated carbon at 400 °C, (c) carbon at 1000 °C, (d) activated carbon at 1000 °C, and (e) AC_{1000°C} MB-0.3:1.

3.1.5. FTIR Analysis

In order to classify the main infrared (IR) bands of organics and determine the adsorption mechanism (physisorption or chemisorption), pure and loaded activated carbon/chitosan microbeads (AC_{400°C} MB-0.3:1 and AC_{1000°C} MB-0.3:1) were investigated by FTIR analysis. Figure 7a,b shows that the bands at 3338 cm⁻¹ and 3299 refer to the bending stretch of the NH₂ group. The peaks observed at 1641 cm⁻¹ and 1639.3 can be attributed to the axial deformation of C=O of the acetamide group, which was assigned to the acetylated part of chitosan. The bands at 1406 cm⁻¹ and 1035 cm⁻¹ are assigned to the angular deformation of C–H of the CH₃ group and to C–O binding and stretching, respectively. These results are close to those recorded for activated carbon/chitosan composites investigated elsewhere [33]. By comparing the two spectra (before and after adsorption), it was noticed that there was no change in the peaks. This means that no chemical bonds were formed within the adsorption process. The change in the peak intensity can be attributed to the electrostatic interaction between the anionic dye molecules and H⁺ ions that accumulated on the activated carbon surface and -NH₂ groups on the surface of the chitosan.

3.1.6. Surface Area

As shown in Figure 8, the BET surface area analysis was conducted in order to investigate the effect of the thermochemical activation process on the adsorption characteristics of carbon particles, such as the surface area and pore volume. The analysis showed that there was a higher improvement in the surface area and pore volume for carbon particles. For carbon at 400 °C, the BET surface area and pore volume increased from 32.5 m²/g and

0.023 cm³/g (before activation) to 99.9 m²/g and 0.037 cm³/g (after activation), respectively. Furthermore, for carbon at 1000 °C, the BET surface area and pore volume increased from 33.1 m²/g and 0.025 cm³/g (before activation) to 138 m²/g and 0.045 cm³/g (after activation), respectively. The results shown in Table 1 indicate that the applied activation process using the HCl solution and microwave radiation gas had a major effect on the BET surface area and pore volume for carbon particles.

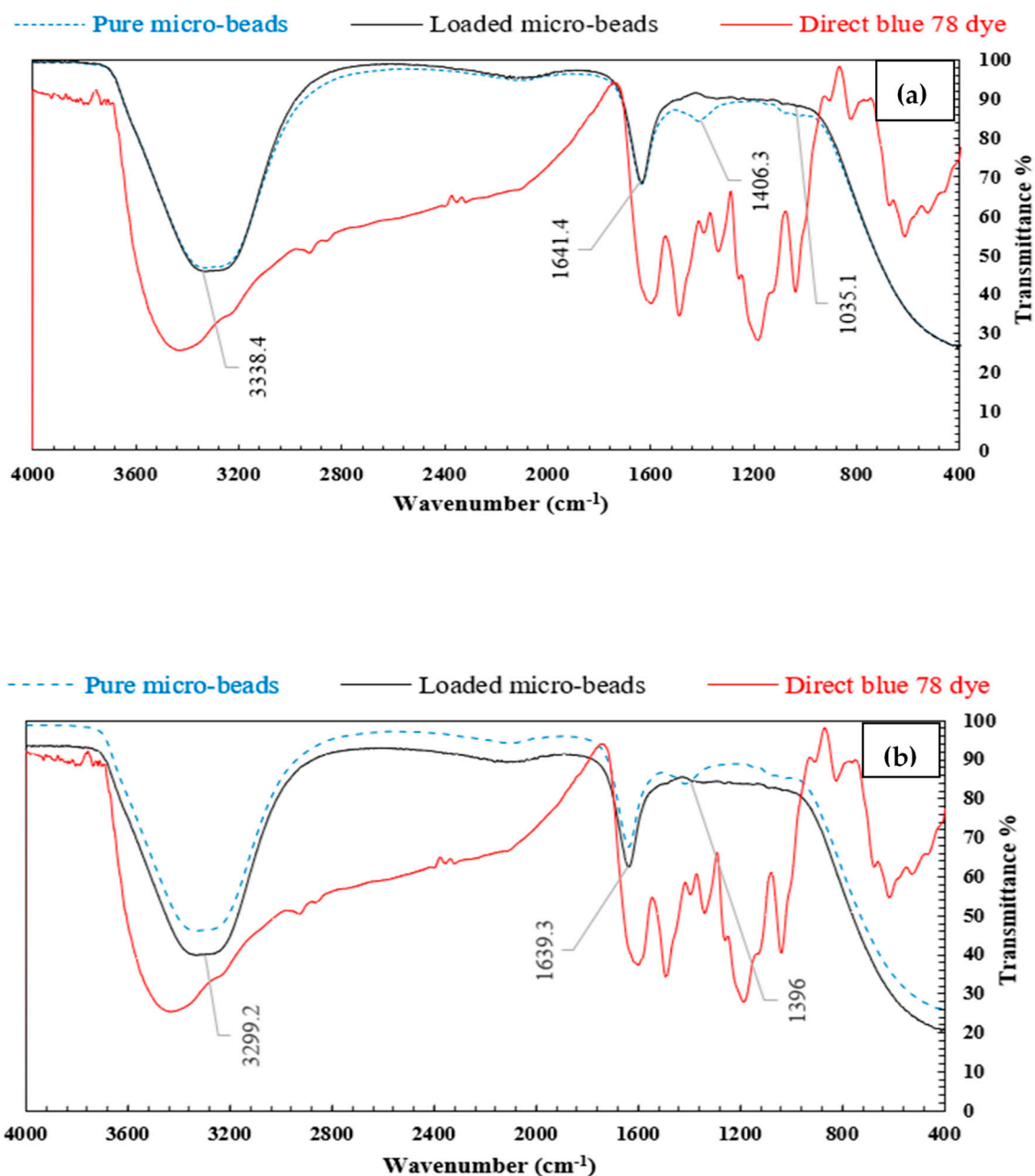


Figure 7. FTIR analysis for neat and loaded (a) AC₄₀₀°C MB-0.3:1 and (b) AC₁₀₀₀°C MB-0.3:1.

Table 1. Adsorption characteristics for carbon samples before and after activation process.

Parameter	C ₄₀₀ °C	AC ₄₀₀ °C	C ₁₀₀₀ °C	AC ₁₀₀₀ °C
Average pore radius (nm)	1.67	1.63	1.78	1.57
BET surface area (m ² /g)	32.59	99.91	33.08	138
Pore volume (cm ³ /g)	0.023	0.037	0.025	0.045

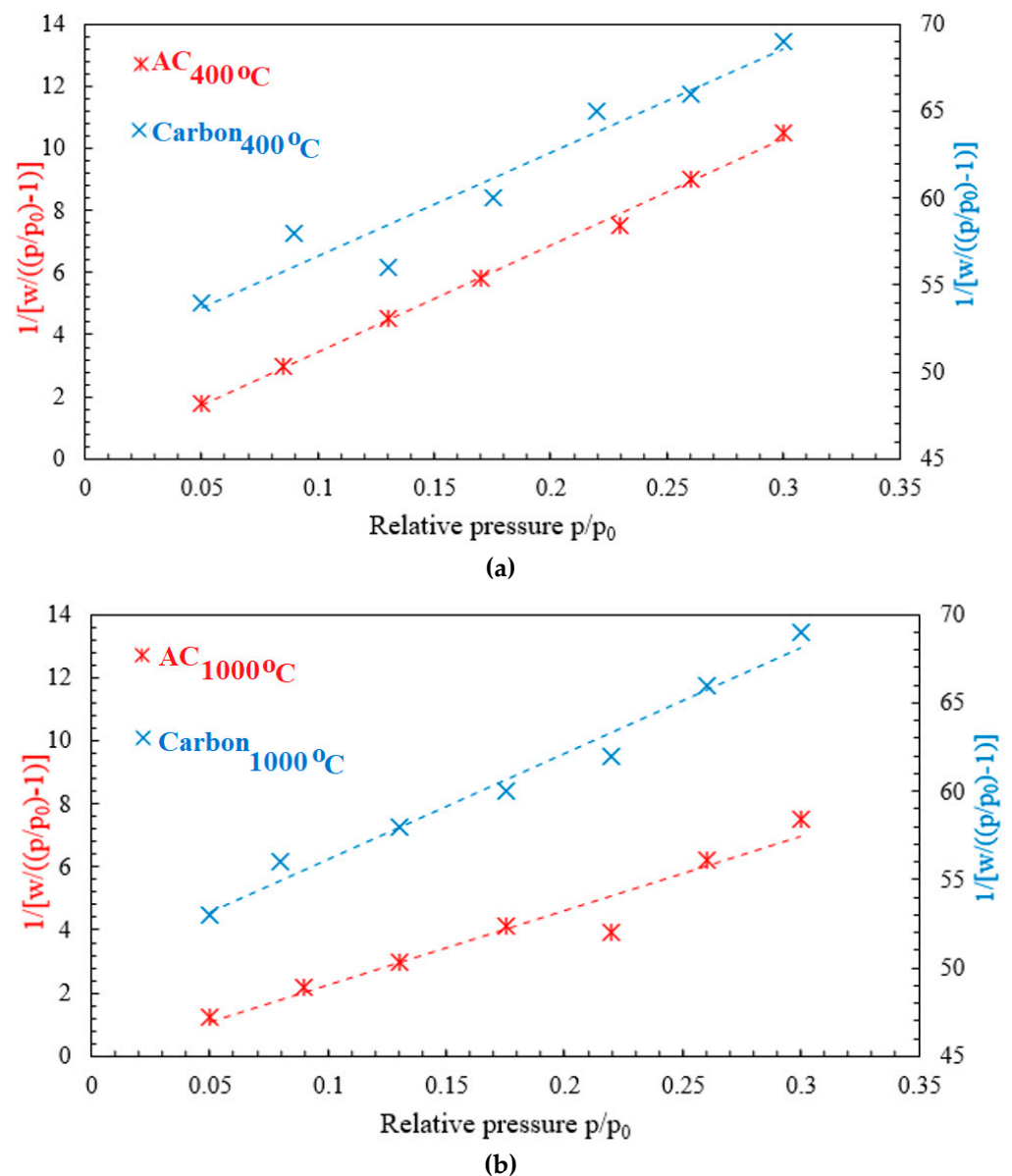


Figure 8. BET analysis for (a) carbon at 400 °C and activated carbon at 400 °C, and (b) carbon at 1000 °C and activated carbon at 1000 °C.

3.2. Adsorption Tests

3.2.1. Effect of Microbead Dose on DB78-Dye-Removal Efficiency

The doses of activated carbon/chitosan microbeads were varied in order to investigate their effects on the efficiency of the direct blue 78 dye removal. It was found that by increasing the microbead dosage (increasing the active adsorption sites), the equilibrium loading decreases and the removal efficiency increases until reaching the maximum efficiency, and then approximately reaches a fixed value. The experiments were conducted by varying the doses of AC_{400 °C} MB-0.3:1 and AC_{1000 °C} MB-0.3:1 from 0.5 to 6.5 g/L. The adsorption process was conducted at initial concentrations of DB78-dye synthetic solutions of 40 mg/L at an ambient temperature of 20 °C, a pH of 4–5, a stirring speed of 200 RPM, and a contact time of 40 min.

Figure 9 demonstrates the influence of the activated carbon/chitosan microbeads on both the dye-removal efficiency (%) and the equilibrium loading (mg/g). For AC_{400 °C} MB-0.3:1, the removal efficiency (97.8%) and equilibrium loading (13.1 mg/g) were obtained by using a AC_{400 °C} MB-0.3:1 dose of 3 g/L for the solution with an initial concentration of

40 mg/L. The maximum equilibrium loading was reached at 31.5 mg/g. It was obtained by using a AC₄₀₀°C MB-0.3:1 dose of 0.5 g/L.

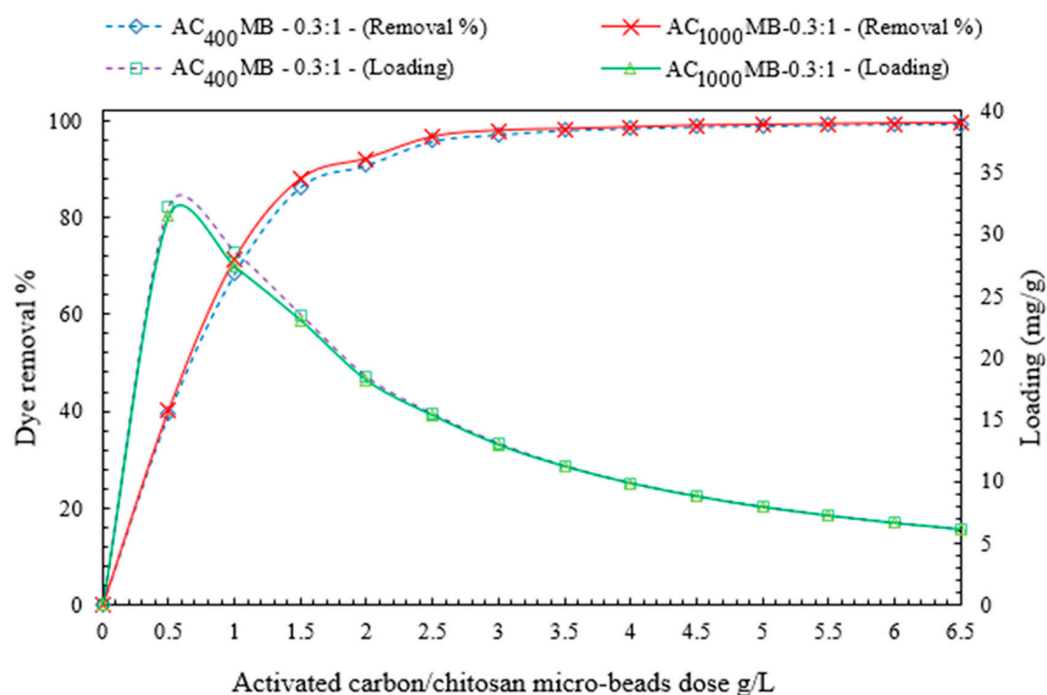


Figure 9. The effects of AC₄₀₀°C MB-0.3:1 and AC₁₀₀₀°C MB-0.3:1 doses on both dye-removal efficiency and equilibrium loading.

Furthermore, for the AC₁₀₀₀°C MB-0.3:1 experimental analysis, the removal efficiency (98.4%) and equilibrium loading (9.85 mg/g) were obtained by using a AC₁₀₀₀°C MB-0.3:1 dose of 4 g/L for the solution with an initial concentration of 40 mg/L. The maximum equilibrium loading reached was 32.2 mg/g. It was obtained by using a AC₁₀₀₀°C MB-0.3:1 dose of 0.5 g/L. It is worth noting that higher q values and lower C_{eq} values indicate that there is less dye in the solution and better adsorption.

3.2.2. Effect of pH on DB78-Dye-Removal Efficiency

The effect of the initial pH of the dye solution was experimentally investigated under a pH range of from 2 to 9. The results are shown in Figure 10. For AC₄₀₀°C MB-0.3:1, the solution pH had a major effect on the chitosan adsorption behavior. AC₄₀₀°C MB-0.3:1 reaches its maximum removal efficiency (97%) under acidic conditions (pH = 5), in comparison with a 92% removal efficiency under alkaline conditions (pH = 9). Moreover, AC₁₀₀₀°C MB-0.3:1 reaches its maximum removal efficiency (96.8%) under acidic conditions (pH = 4), in comparison with an 80% removal efficiency under alkaline conditions (pH = 9). The experiments were conducted under the following conditions: a temperature of 20 °C, a mixing speed of 200 RPM, a microbead dose of 3 g/L, and a contact time of 40 min. These results could be attributed to the major presence of hydrogen ions (H⁺) in the solution under acidic conditions. These ions accumulated on the activated carbon particles and improved their surface positive charge. This improvement in the surface charge increases the ability of activated carbon particles to attract the anionic molecules of direct blue 78 dye.

In addition, the swelling of chitosan powder into chitosan beads in the presence of acidic conditions will protonate the amine groups (NH₂) into NH₃⁺. This process will improve the electrostatic interaction between chitosan particles and dye ions, and enhance the activated carbon/chitosan microbead ability for anionic-dye removal.

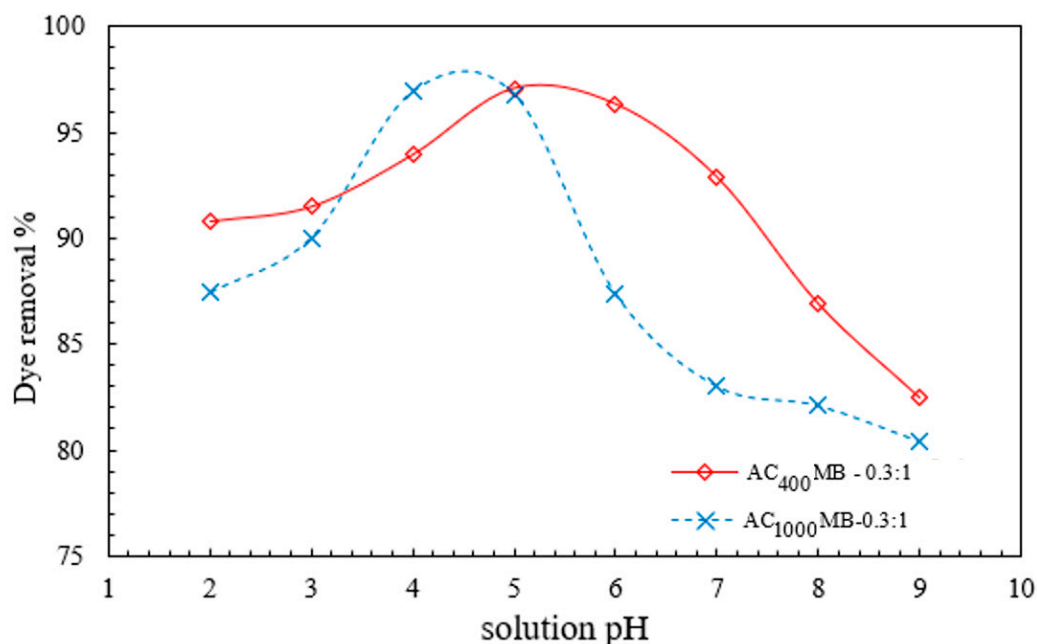


Figure 10. The effect of pH on DB78-dye-removal efficiency using AC₄₀₀°C MB-0.3:1 and AC₁₀₀₀°C MB-0.3:1.

3.2.3. Effect of Contact Time on DB78-Dye-Removal Efficiency

Figure 11 shows the influence of the contact time on the dye-removal efficiency and equilibrium loading. It was experimentally observed that the percentage of dye removal increases with the increase in the contact time. At a specific time, the microbead reached its maximum loading capacity (equilibrium loading q_e). At contact time (50 min) and the AC₁₀₀₀°C MB-0.3:1 dose (3 g/L), the equilibrium concentration decreased to 1.1 mg/L, with a dye-removal efficiency of 97%, and an optimum loading capacity of 9.7 mg/g for an initial dye concentration of 40 mg/L. These experiments were conducted under the following conditions: a temperature of 20 °C and a rate of mixing of 200 RPM.

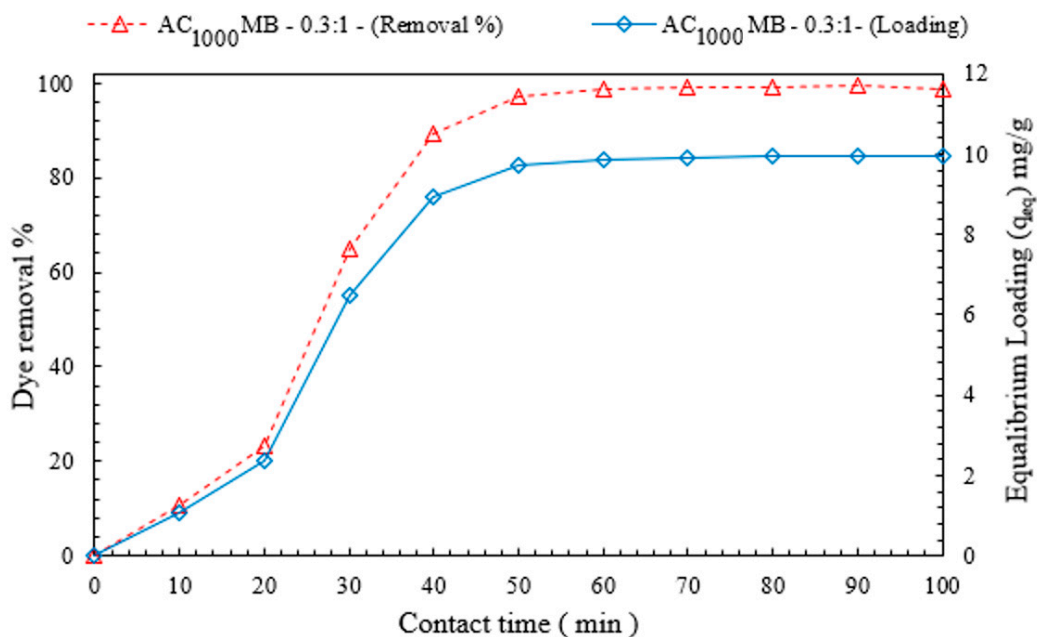


Figure 11. The effect of contact time on both DB78-dye-removal efficiency and equilibrium loading.

3.2.4. Effect of Activated Carbon/Chitosan Ratio on DB78 Dye Removal

To study the composition of the microbead production on the DB78-dye-removal efficiency, different ratios of AC and chitosan were applied (e.g., ACMB-0.1:1, ACMB-0.2:1, ACMB-0.3:1, ACMB-0.4:1, and ACMB-0.5:1). The initial dye concentration was 40 mg/L, the pH range was 4:5, the contact time was 40 min, the microbead dose was 3 g/L, and the stirrer speed was 200 RPM. The experimental results show that the dye-removal efficiency increases with the increase in the activated carbon loading up to 0.3:1. No significant improvement in the dye removal was found at higher activated carbon loads, as is shown in Figure 12. This can be attributed to a blockage of the internal porosities of chitosan by the incorporation of higher activated carbon loadings. Figure 13 shows the DB78 dye solution and dye removal using AC_{400°C} MB-0.3:1 and AC_{1000°C} MB-0.3:1. It was observed that there was a slight improvement in the efficiency of the dye removal using AC_{1000°C} compared with AC_{400°C}. This result is in a good agreement with the EDX analysis, as a higher carbon content (97.4%) was found in the activated carbon produced at 1000 °C.

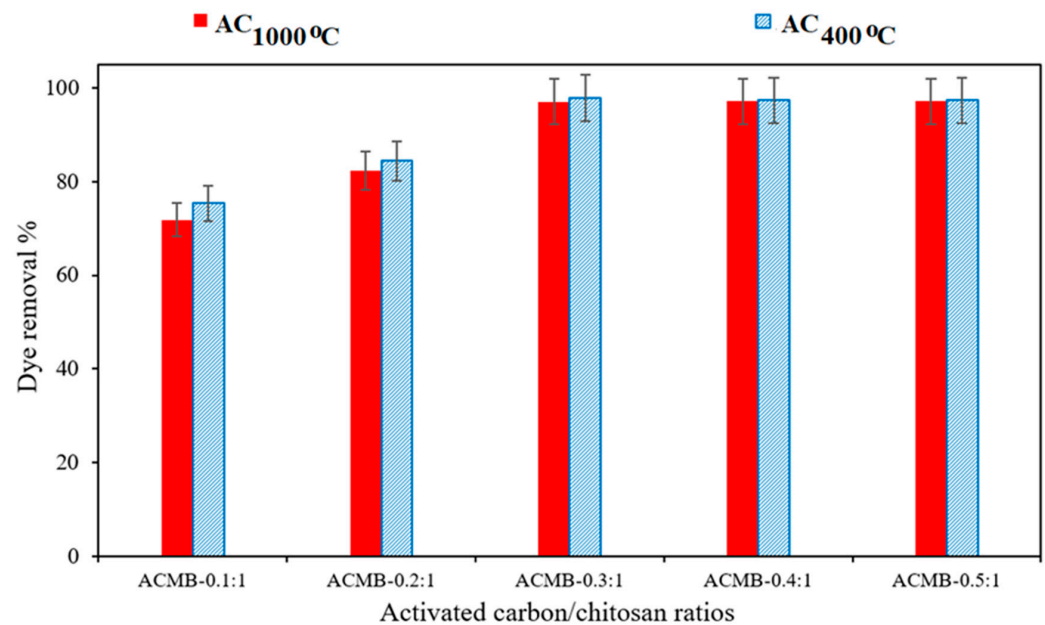


Figure 12. The effect of activated carbon/chitosan ratios on DB78-dye-removal efficiency.



Figure 13. DB78 dye solution and dye removal using AC_{1000°C} MB-0.3:1 and AC_{400°C} MB-0.3:1.

3.2.5. Effect of Contact Time

The influence of the contact time on the dye removal percentage and adsorbent loading was studied. The percentage of dye removed increased with the increase in the mixing time until the maximum removal efficiency was reached, as is illustrated in Figure 14. The adsorbent achieved its maximum loading capacity at this point (equilibrium loading q_{eq}). For a dye concentration of 40 mg/L of solution, a contact time of 50 min, and a 3 g/L adsorbent dose of AC_{1000°C} MB-0.3:1, the dye-removal efficiency was 99%, and the optimal loading capacity was 10 mg/g. When comparing AC_{1000°C} MB-0.3:1 with AC_{400°C} MB-3:1, a slight improvement in the dye removal was observed. This could be due to the AC_{1000°C} MB-3's increased carbon content.

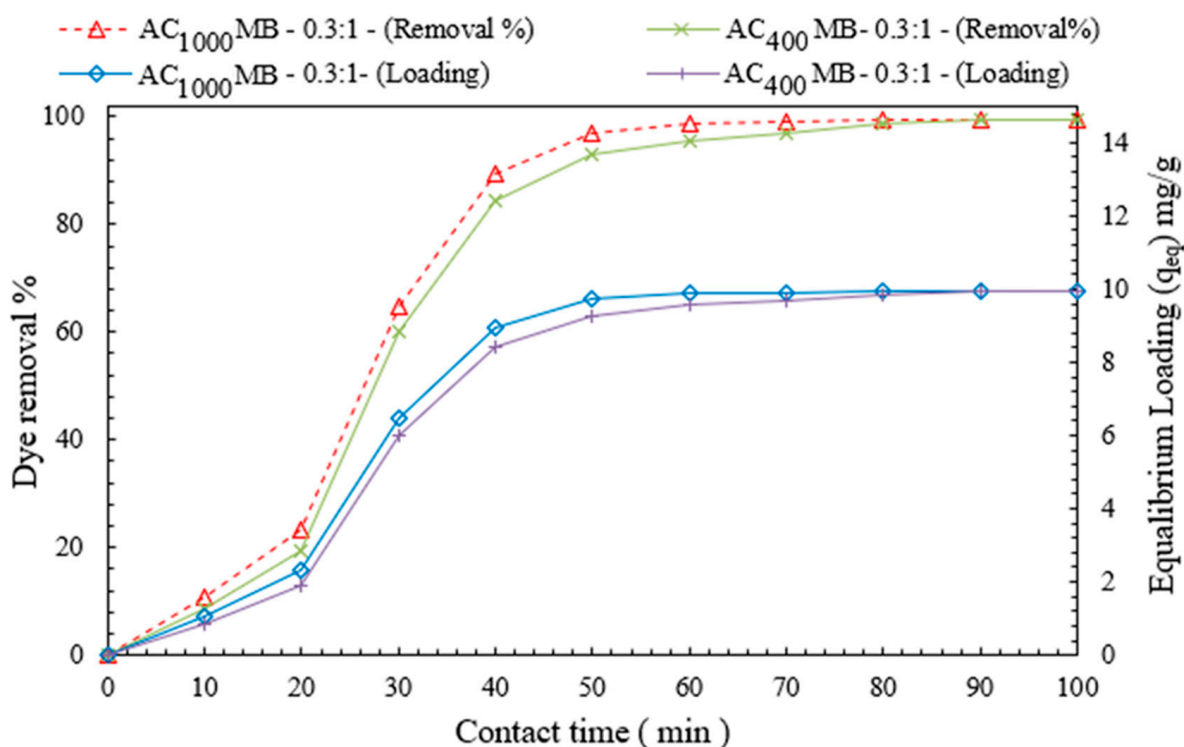


Figure 14. Effect of contact time on dye removal.

3.3. Adsorption Isotherm

Figure 15 shows the adsorption isothermal curve. It indicates the amount of adsorbate (DB78 dye) by the activated carbon/chitosan microbead (AC_{400°C} MB-0.3:1 and AC_{1000°C} MB-0.3:1) q_{eq} against the adsorbate concentration in the liquid state (C_{eq}). The initial concentration was 40 mg/L. These results are essential considerations in the design of adsorption systems. Moreover, the form of the equilibrium curve helps to describe other phenomena that are linked with the adsorption mechanism. The equilibrium curves are identified under four main classes according to the primary slope and subgroups that are described for each class based on the upper-part shapes and slope changes: (a) S curves, or vertical-orientation isotherms; (b) L curves, or normal or “Langmuir” isotherms; (c) H curves, or high-affinity isotherms; and (d) C curves, or constant-partition isotherms [34].

The initial shape of the equilibrium curve (L shape) in Figure 15 follows the basic premise that the higher the solute concentration, the greater the adsorption capacity, until the number of the adsorption site clearance is limited, and competition occurs between the solute molecules for the available sites. This isotherm type indicates that the adsorption occurs due to relatively weak forces, such as “van der Waals forces”. Several isothermal models (equations) are available, and the two important isotherms are selected in this study, which are, namely, the Freundlich and Langmuir isotherms.

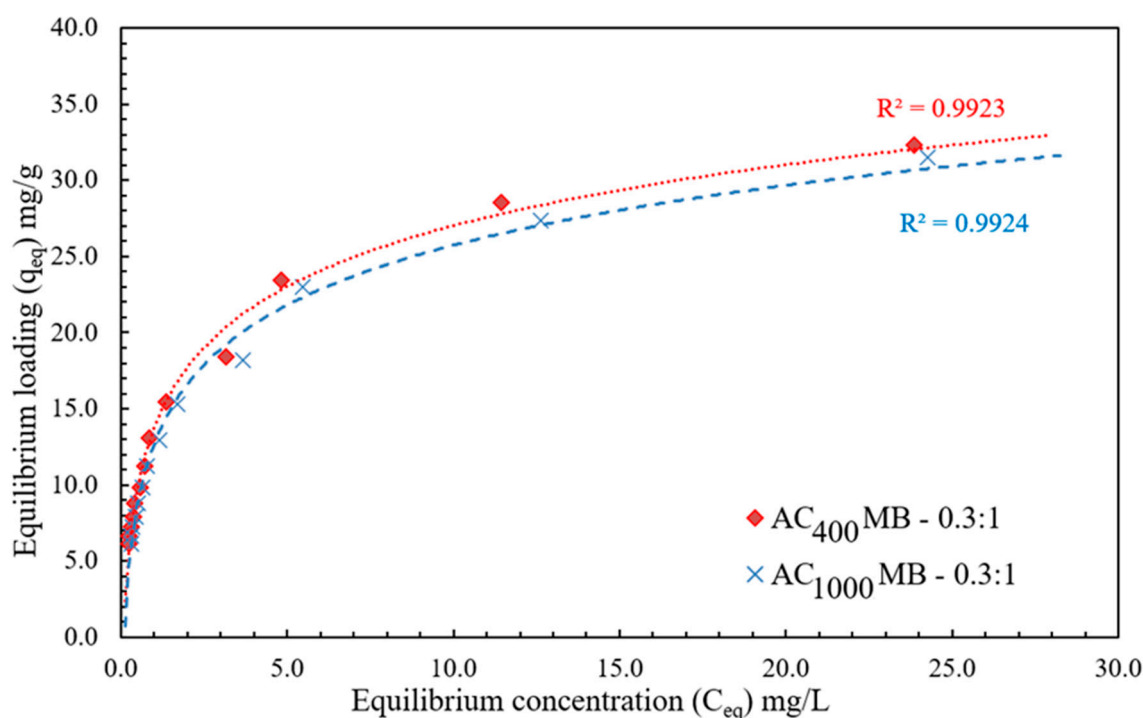


Figure 15. The adsorption isotherm for DB78 dye removal using AC₄₀₀°C MB-0.3:1 and AC₁₀₀₀°C MB-0.3:1.

The Freundlich isotherm refers to the adsorption on a heterogeneous surface, and the adsorbed mass increased exponentially with an increase in the concentration [35]. This isotherm explains the equilibrium on heterogeneous surfaces and, hence, the capacity is not a presumed monolayer. In the liquid phase, this isotherm is given by Equation (3):

$$Q_e = K_f C_e^{n_f} \quad (3)$$

where k_f is the Freundlich fixed value (k_f unit = mg/g, where n_f is the Freundlich exponent). This isotherm focused on integrating the role of the adsorbent (adsorbate–surface interactions). Figure 16 shows the application of equilibrium data according to the Freundlich isotherm. For AC₄₀₀°C MB-0.3:1, the Freundlich constant (k_f) value was 11.86, and the heterogeneity factor ($1/n_f$) value was 0.36 for the solution with an initial concentration of 40 mg/L. For AC₁₀₀₀°C MB-0.3:1, the Freundlich constant (k_f) value was 11.13 mg/L, and the heterogeneity factor ($1/n_f$) value was 0.37 for an initial concentration 40 mg/L. The Freundlich equation's (n_f) parameter was used to subjectively test the adsorption intensity, revealing the adsorbent's affinity for the dye removal, and suggesting good adsorption when it had values greater than 1.

The Langmuir isotherm believes that sorption occurs within the adsorbent at different homogeneous sites. It has been successfully applied to several processes of sorption. The isotherm's physical simplicity is based on some assumptions: Adsorption cannot occur beyond the monolayer coverage. Each site can hold only one adsorbate molecule. All sites are energetically equivalent. The surface is uniform. The linear form of the Langmuir isotherm is given by the following equation, Equation (4):

$$(C_e/q_e) = (1/Q_0 b) + (C_e/Q_0) \quad (4)$$

where C_e is the equilibrium concentration (mg/L), q_e is the mass adsorbed at equilibrium (mg/g), Q_0 is the adsorbent loading (mg/g), and b is the adsorption energy (Langmuir fixed value of L/mg). The values of Q_0 and b were determined from the slope and intercept of the linear plots' C_e/q_e versus C_e , respectively, which resulted in a straight line of slope

$1/Q_0$ corresponding to the total coverage of the monolayer (mg/g), and the intercept is $1/Q_0b$ [36].

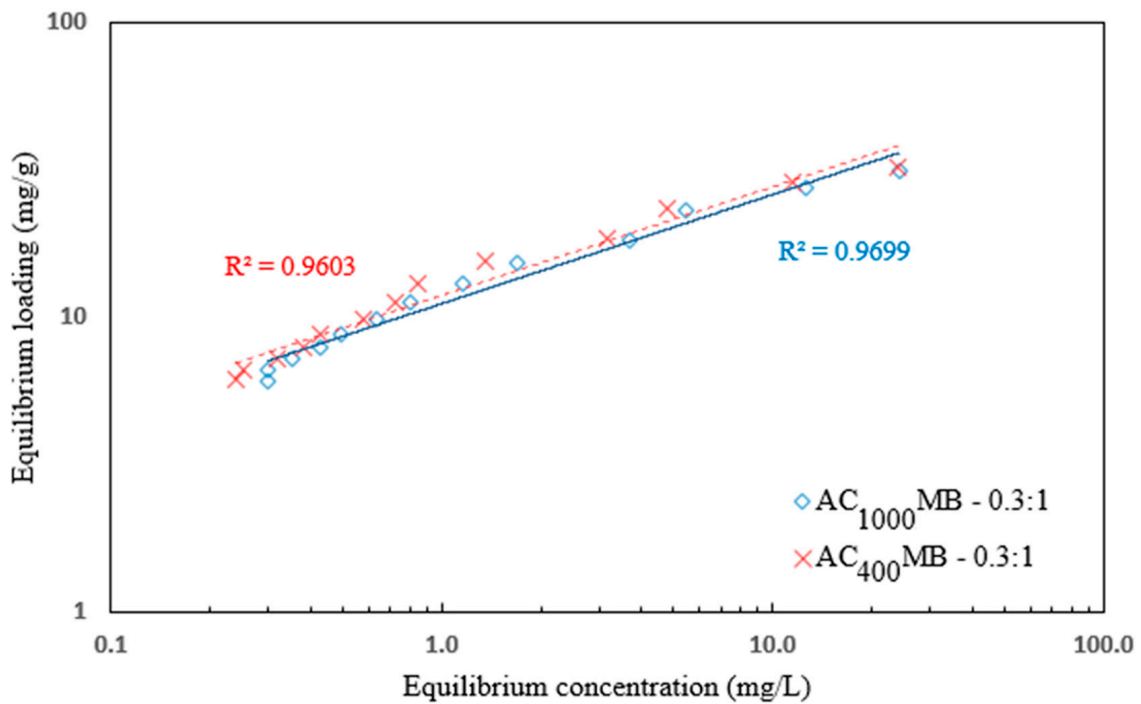


Figure 16. Freundlich isotherm for DB78 dye removal using AC₄₀₀°C MB-0.3:1 and AC₁₀₀₀°C MB-0.3:1.

Figure 17 shows the application of equilibrium data according to the Langmuir isotherm. For AC₄₀₀°C MB-0.3:1, the adsorbent loading value (Q_0) was 33.5 mg/g. The Langmuir fixed value (b) was 1.47 L/mg for an initial concentration of 40 mg/L. For AC₁₀₀₀°C MB-0.3:1, the adsorbent loading value (Q_0) was 32.8 mg/g, and the Langmuir fixed value (b) was 1.68 L/mg. It is observed from the listed adsorption isothermal models in Table 2 that the adsorption of the DB78 dye using both AC₄₀₀°C MB-0.3:1 and AC₁₀₀₀°C MB-0.3:1 followed the Langmuir isotherm.

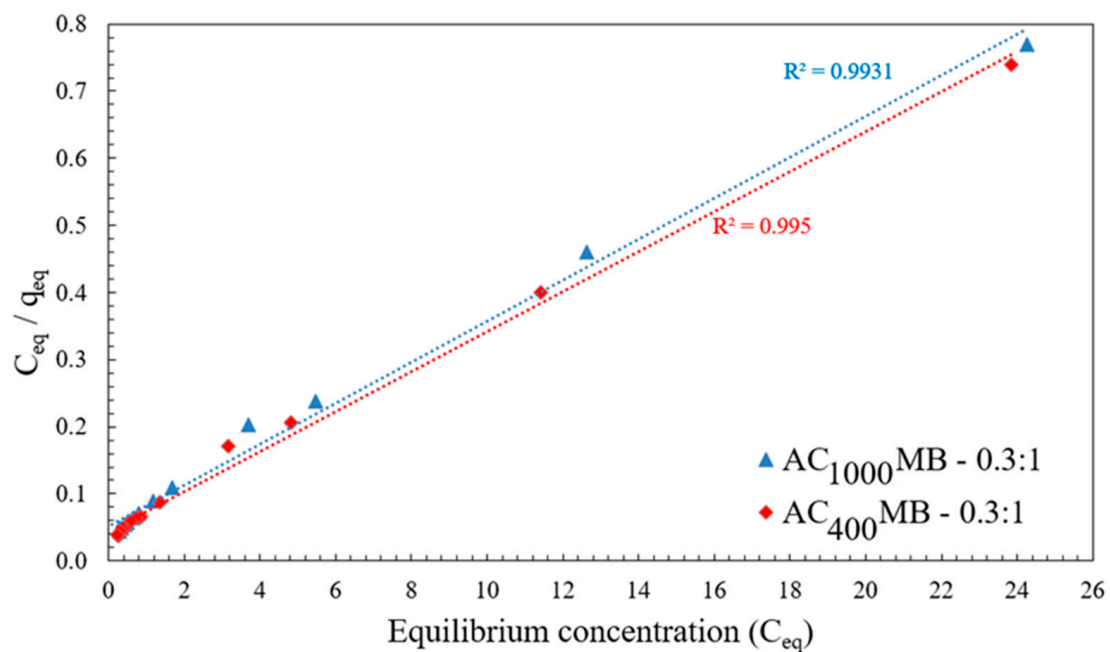


Figure 17. Langmuir isotherm for DB78 dye removal using AC₄₀₀°C MB-0.3:1 and AC₁₀₀₀°C MB-0.3:1.

Table 2. Comparison of adsorption isothermal models for adsorbents (AC_{400°C} MB-0.3:1 and AC_{1000°C} MB-0.3:1).

Freundlich Isothermal			Langmuir Isothermal			Adsorbent
R ²	1/n	K _f (mg/g)	R ²	B (L/mg)	Q ₀ (mg/g)	
0.960	0.36	11.86	0.995	1.47	33.5	AC _{400°C} MB-0.3:1
0.969	0.37	11.13	0.993	1.68	32.7	AC _{1000°C} MB-0.3:1

3.4. Adsorption Kinetics

In order to understand the mechanism of the adsorption process, kinetic studies were conducted by analyzing the samples at time intervals of 10 min until the consecutive residue dye concentrations became closer. The kinetic data for the adsorption process of the DB78 dyes AC_{400°C} MB-0.3:1 and AC_{1000°C} MB-0.3:1, with initial dye concentrations of 40 mg/L, were examined with the well-known kinetic models: the pseudo first-order model (PFO) and pseudo second-order model (PSO). The plotting of these kinetic models is shown in Figure 18.

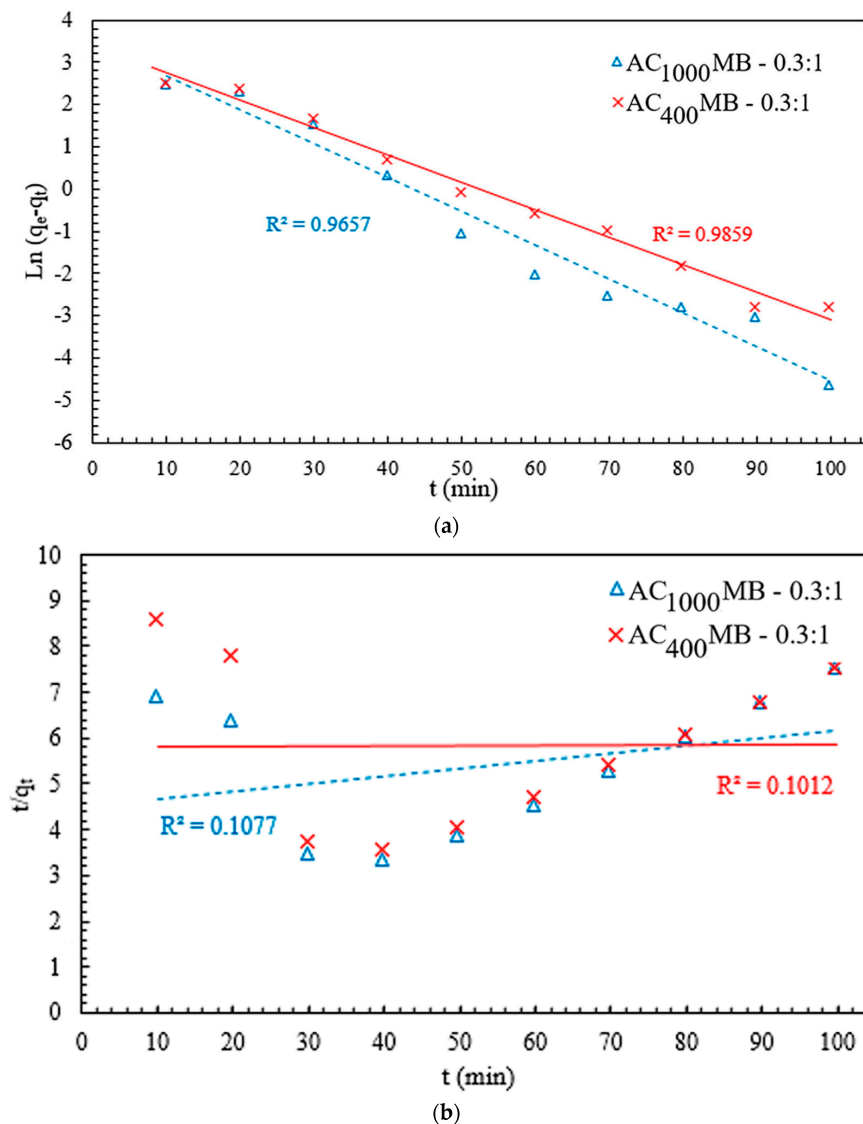


Figure 18. Adsorption kinetic studies: (a) pseudo first-order model and (b) pseudo second-order model.

The pseudo first-order equation.

The pseudo first-order kinetic equation was used for the adsorption analysis. The linear form of this equation is:

$$\ln (q_e - q_t) = \ln q_e - k_1 t \quad (5)$$

where q_e (mg/g) and q_t (mg/g) are the amounts of adsorbed adsorbate at equilibrium and at time (t), respectively, and K_1 (min^{-1}) is the rate constant of the pseudo first-order model.

The pseudo second-order equation.

The adsorption kinetics can also be described by the pseudo second-order model. The linear form of the pseudo second-order equation is expressed as:

$$(t/q_t) = (1/k_2 q_e^2) + (1/q_e) t \quad (6)$$

where k_2 (g/mg min) is the equilibrium rare constant of the pseudo second-order adsorption, where q_e (mg/g) and q_t (mg/g) are the amounts of adsorbed adsorbate at equilibrium and at time (t), respectively.

Figure 18 shows the linear plots of the PFO and PSO models of $\text{AC}_{400^\circ\text{C}}$ MB-0.3:1 and $\text{AC}_{1000^\circ\text{C}}$ MB-0.3:1. The kinetic parameters are listed in Table 3. On the basis of the low correlation coefficient for the PSO and the high value for the PFO, the adsorption abilities of $\text{AC}_{400^\circ\text{C}}$ MB-0.3:1 and $\text{AC}_{1000^\circ\text{C}}$ MB-0.3:1 follow the PFO rather than the PSO. These results suggest that, for $\text{AC}_{400^\circ\text{C}}$ MB-0.3:1, the PFO can best predict the kinetic process. The value of $q_e = 29.5$ mg/g calculated by the PFO was more similar to the practical $q_e = 9.76$ mg/g than the PSO. For $\text{AC}_{1000^\circ\text{C}}$ MB-0.3:1, the PFO can best predict the kinetic process. The value of $q_e = 32.4$ mg/g calculated by the PFO was more similar to the practical $q_e = 9.96$ mg/g than the PSO, as listed in Table 3. For $\text{AC}_{400^\circ\text{C}}$ MB-0.3:1 and $\text{AC}_{1000^\circ\text{C}}$ MB-0.3:1, the applicability of the PFO model indicates the interaction between the dye molecules and the microbead surface. Hence, the adsorption system is physical adsorption [37].

Table 3. Kinetic model parameters.

Kinetic Model Parameters	Pseudo First-Order Model			Pseudo Second-Order Model		
	K_1 (1/min)	q_e (mg/g)	R^2	K_2 (g/mg min)	q_e (mg/g)	R^2
$\text{AC}_{400^\circ\text{C}}$ MB-0.3:1	0.065	29.5	0.985	5.2×10^{-5}	57.66	0.101
$\text{AC}_{1000^\circ\text{C}}$ MB-0.3:1	0.08	32.45	0.965	6.11×10^{-5}	60.24	0.107

4. Conclusions

The removal of anionic dye (DB78) from synthetic wastewater by adsorption onto novel activated carbon/chitosan microbeads ($\text{AC}_{400^\circ\text{C}}$ MB and $\text{AC}_{1000^\circ\text{C}}$ MB) was experimentally studied. Several microbeads with different activated carbon/chitosan ratios (0.1:1, 0.2:1, 0.3:1, 0.4:1, and 0.5:1) were synthesized in order to study the effect of the activated carbon quantity on the removal efficiency. It was observed that the removal efficiency increases with the increasing activated carbon quantity in synthetic microbeads up to a ratio of 0.3:1. The adsorption process is highly dependent on the solution pH, and the ACMB reaches its maximum equilibrium loading under acidic conditions (pH = 4.5). Based on the experimental results, it was observed that the removal efficiencies of 97.8% and 98.4% were obtained by using the adsorbents $\text{AC}_{400^\circ\text{C}}$ MB-0.3:1 and $\text{AC}_{1000^\circ\text{C}}$ MB-0.3:1, respectively, with initial concentrations of 40 mg/L. The equilibrium studies show that the initial shape of the equilibrium curve is an L shape, which means that the adsorption process resulted from the electrostatic interaction between the dye molecules and the adsorbent particles (physical forces). The adsorption studies were studied by using the Langmuir and Freundlich isothermal models, and the results were best fit to the Langmuir

isotherm. Therefore, AC_{400°C} MB-0.3:1 and AC_{1000°C} MB-0.3:1 could be highly efficient sorbents for the removal of anionic contaminants. The thermochemical method using microwave radiation and an HCl solution resulted in promising dye adsorbents for textile wastewater treatment.

Author Contributions: Conceptualization, H.H.S., M.B., A.H., R.K., I.A., B.V.A. and Y.E.; methodology, H.H.S., M.B., R.K., I.A., B.V.A. and Y.E.; validation, H.H.S., M.B., R.K., I.A., B.V.A. and Y.E.; formal analysis H.H.S., M.B., R.K., I.A., B.V.A. and Y.E.; investigation, H.H.S., M.B., R.K., I.A., B.V.A. and Y.E.; resources, H.H.S., M.B., A.H., R.K., I.A., B.V.A. and Y.E.; data curation, H.H.S., M.B., R.K., I.A., B.V.A. and Y.E.; writing—M.B. and Y.E.; writing—review and editing, H.H.S., M.B., R.K., I.A., B.V.A. and Y.E.; visualization, H.H.S., M.B., R.K., I.A., B.V.A. and Y.E.; supervision, H.H.S., M.B., R.K., I.A., B.V.A. and Y.E.; project administration, H.H.S., M.B., A.H., R.K., I.A., B.V.A. and Y.E.; funding acquisition, H.H.S., M.B., A.H., R.K., I.A., B.V.A. and Y.E. All authors have read and agreed to the published version of the manuscript.

Funding: This research was funded by the National plan for Science, Technology, and Innovation (MAARIFAH), King Abdulaziz City for Science and Technology, The Kingdom of Saudi Arabia, Award No. 11-WAT2033-03. The authors also acknowledge with thanks the staff at the Science and Technology Unit of King Abdulaziz University in Jeddah for their technical support.

Institutional Review Board Statement: Not applicable.

Informed Consent Statement: Not applicable.

Data Availability Statement: No new data were created or analyzed in this study. Data sharing is not applicable to this article.

Conflicts of Interest: The authors declare no conflict of interest.

References

1. Rai, P.; Gautam, R.K.; Banerjee, S.; Rawat, V.; Chattopadhyaya, M.C. Synthesis and characterization of a novel SnFe₂O₄@ activated carbon magnetic nanocomposite and its effectiveness in the removal of crystal violet from aqueous solution. *J. Environ. Chem. Eng.* **2015**, *3*, 2281–2291. [[CrossRef](#)]
2. Shirsath, S.R.; Patil, A.P.; Bhanvase, B.A.; Sonawane, S.H. Ultrasonically prepared poly (acrylamide)-kaolin composite hydrogel for removal of crystal violet dye from wastewater. *J. Environ. Chem. Eng.* **2015**, *3*, 1152–1162. [[CrossRef](#)]
3. Kubra, K.T.; Salman, M.S.; Znad, H.; Hasan, M.N. Efficient encapsulation of toxic dye from wastewater using biodegradable polymeric adsorbent. *J. Mol. Liq.* **2021**, *329*, 115541. [[CrossRef](#)]
4. Foroutan, R.; Peighambaroust, S.J.; Esvandi, Z.; Khatooni, H.; Ramavandi, B. Evaluation of two cationic dyes removal from aqueous environments using CNT/MgO/CuFe₂O₄ magnetic composite powder: A comparative study. *J. Environ. Chem. Eng.* **2021**, *9*, 104752. [[CrossRef](#)]
5. Cheruiyot, G.K.; Wanyonyi, W.C.; Kiplimo, J.J.; Maina, E.N. Adsorption of toxic crystal violet dye using coffee husks: Equilibrium, kinetics and thermodynamics study. *Sci. Afr.* **2019**, *5*, e00116. [[CrossRef](#)]
6. Foroutan, R.; Peighambaroust, S.J.; Aghdasinia, H.; Mohammadi, R.; Ramavandi, B. Modification of bio-hydroxyapatite generated from waste poultry bone with MgO for purifying methyl violet-laden liquids. *Environ. Sci. Pollut. Res.* **2020**, *27*, 44218–44229. [[CrossRef](#)]
7. Peighambaroust, S.J.; Aghamohammadi-Bavil, O.; Foroutan, R.; Arsalani, N. Removal of malachite green using carboxymethyl cellulose-g-polyacrylamide/montmorillonite nanocomposite hydrogel. *Int. J. Biol. Macromol.* **2020**, *159*, 1122–1131. [[CrossRef](#)]
8. Eteba, A.; Bassyouni, M.; Saleh, M. Removal of Hazardous Organic Pollutants Using Fly Ash. *Environ. Ecol. Res.* **2021**, *9*, 196–203. [[CrossRef](#)]
9. Lellis, B.; Fávoro-Polonio, C.Z.; Pamphile, J.A.; Polonio, J.C. Effects of textile dyes on health and the environment and bioremediation potential of living organisms. *Biotechnol. Res. Innov.* **2019**, *3*, 275–290. [[CrossRef](#)]
10. El-Mehalmey, W.A.; Safwat, Y.; Bassyouni, M.; Alkordi, M.H. Strong interplay between polymer surface charge and MOF cage chemistry in mixed-matrix membrane for water treatment applications. *ACS Appl. Mater. Interfaces* **2020**, *12*, 27625–27631. [[CrossRef](#)]
11. Fouad, K.; Alalm, M.G.; Bassyouni, M.; Saleh, M.Y. A novel photocatalytic reactor for the extended reuse of W-TiO₂ in the degradation of sulfamethazine. *Chemosphere* **2020**, *257*, 127270. [[CrossRef](#)] [[PubMed](#)]
12. Abdel-Aziz, M.H.; El-Ashtoukhy, E.Z.; Zoromba, M.S.; Bassyouni, M.; Sedahmed, G.H. Removal of nitrates from water by electrocoagulation using a cell with horizontally oriented Al serpentine tube anode. *J. Ind. Eng. Chem.* **2020**, *82*, 105–112. [[CrossRef](#)]
13. Abdel-Aziz, M.H.; Bassyouni, M.; Zoromba, M.S.; Alshehri, A.A. Removal of dyes from waste solutions by anodic oxidation on an array of horizontal graphite rods anodes. *Ind. Eng. Chem. Res.* **2018**, *58*, 1004–1018. [[CrossRef](#)]

14. Bassyouni, M.; Mansi, A.E.; Elgabry, A.; Ibrahim, B.A.; Kassem, O.A.; Alhebeshy, R. Utilization of carbon nanotubes in removal of heavy metals from wastewater: A review of the CNTs' potential and current challenges. *Appl. Phys. A* **2020**, *126*, 38. [[CrossRef](#)]
15. Elhenawy, Y.; Elminshawy, N.A.; Bassyouni, M.; Alanezi, A.A.; Drioli, E. Experimental and theoretical investigation of a new air gap membrane distillation module with a corrugated feed channel. *J. Membr. Sci.* **2020**, *594*, 117461. [[CrossRef](#)]
16. Liu, L.; Li, S.; Zheng, J.; Bu, T.; He, G.; Wu, J. Safety considerations on food protein-derived bioactive peptides. *Trends Food Sci. Technol.* **2020**, *96*, 199–207. [[CrossRef](#)]
17. Liu, Q.; Li, Y.; Chen, H.; Lu, J.; Yu, G.; Möslang, M.; Zhou, Y. Superior adsorption capacity of functionalised straw adsorbent for dyes and heavy-metal ions. *J. Hazard. Mater.* **2020**, *382*, 121040. [[CrossRef](#)]
18. Mezohegyi, G.; van der Zee, F.P.; Font, J.; Fortuny, A.; Fabregat, A. Towards advanced aqueous dye removal processes: A short review on the versatile role of activated carbon. *J. Environ. Manag.* **2012**, *102*, 148–164. [[CrossRef](#)]
19. Vakili, M.; Rafatullah, M.; Salamatinia, B.; Abdullah, A.Z.; Ibrahim, M.H.; Tan, K.B.; Gholami, Z.; Amouzgar, P. Application of chitosan and its derivatives as adsorbents for dye removal from water and wastewater: A review. *Carbohydr. Polym.* **2014**, *113*, 115–130. [[CrossRef](#)]
20. Crini, G.; Lichtfouse, E.; Wilson, L.D.; Morin-Crini, N. Conventional and non-conventional adsorbents for wastewater treatment. *Environ. Chem. Lett.* **2019**, *17*, 195–213. [[CrossRef](#)]
21. Pintar, A. Catalytic processes for the purification of drinking water and industrial effluents. *Catal. Today* **2003**, *77*, 451–465. [[CrossRef](#)]
22. El-Sheikh, A.H.; Newman, A.P.; Al-Daffae, H.K.; Phull, S.; Cresswell, N. Characterization of activated carbon prepared from a single cultivar of Jordanian Olive stones by chemical and physicochemical techniques. *J. Anal. Appl. Pyrolysis* **2004**, *71*, 151–164. [[CrossRef](#)]
23. Hesas, R.H.; Daud, W.M.A.W.; Sahu, J.N.; Arami-Niya, A. The effects of a microwave heating method on the production of activated carbon from agricultural waste: A review. *J. Anal. Appl. Pyrolysis* **2013**, *100*, 1–11. [[CrossRef](#)]
24. Li, W.; Peng, J.; Zhang, L.; Yang, K.; Xia, H.; Zhang, S.; Guo, S.H. Preparation of activated carbon from coconut shell chars in pilot-scale microwave heating equipment at 60 kW. *Waste Manag.* **2009**, *29*, 756–760. [[CrossRef](#)] [[PubMed](#)]
25. Guo, Y.; Zhao, J.; Zhang, H.; Yang, S.; Qi, J.; Wang, Z.; Xu, H. Use of rice husk-based porous carbon for adsorption of Rhodamine B from aqueous solutions. *Dyes Pigments* **2005**, *66*, 123–128. [[CrossRef](#)]
26. Tan, I.A.W.; Ahmad, A.L.; Hameed, B.H. Optimization of preparation conditions for activated carbons from coconut husk using response surface methodology. *Chem. Eng. J.* **2008**, *137*, 462–470. [[CrossRef](#)]
27. Tan, I.A.W.; Hameed, B.H.; Ahmad, A.L. Equilibrium and kinetic studies on basic dye adsorption by oil palm fibre activated carbon. *Chem. Eng. J.* **2007**, *127*, 111–119. [[CrossRef](#)]
28. Szymańska, E.; Winnicka, K. Stability of chitosan—A challenge for pharmaceutical and biomedical applications. *Mar. Drugs* **2015**, *13*, 1819–1846. [[CrossRef](#)]
29. Ruan, C.Q.; Strømme, M.; Lindh, J. Preparation of porous 2, 3-dialdehyde cellulose beads crosslinked with chitosan and their application in adsorption of Congo red dye. *Carbohydr. Polym.* **2018**, *181*, 200–207. [[CrossRef](#)]
30. Chiu, C.-W.; Wu, M.-T.; Lee, J.C.-M.; Cheng, T.-Y. Isothermal adsorption properties for the adsorption and removal of reactive blue 221 dye from aqueous solutions by cross-linked β -chitosan glycan as acid-resistant adsorbent. *Polymers* **2018**, *10*, 1328. [[CrossRef](#)]
31. Sait, H.H.; Hussain, A.; Bassyouni, M.; Ali, I.; Kanthasamy, R.; Ayodele, B.V.; Elhenawy, Y. Hydrogen-Rich Syngas and Biochar Production by Non-Catalytic Valorization of Date Palm Seeds. *Energies* **2022**, *15*, 2727. [[CrossRef](#)]
32. Ahmaruzzaman, M. Adsorption of phenolic compounds on low-cost adsorbents: A review. *Adv. Colloid Interface Sci.* **2008**, *143*, 48–67. [[CrossRef](#)] [[PubMed](#)]
33. de Freitas, F.P.; Carvalho, A.M.M.L.; Carneiro, A.D.C.O.; de Magalhães, M.A.; Xisto, M.F.; Canal, W.D. Adsorption of neutral red dye by chitosan and activated carbon composite films. *Heliyon* **2021**, *7*, e07629. [[CrossRef](#)]
34. Nasir, M.; Hashim, R.; Sulaiman, O.; Nordin, N.A.; Lamaming, J.; Asim, M. Laccase, an emerging tool to fabricate green composites: A review. *BioResources* **2015**, *10*, 6262–6284. [[CrossRef](#)]
35. Abraham, E.; Deepa, B.; Pothan, L.A.; Jacob, M.; Thomas, S.; Cvelbar, U.; Anandjiwala, R. Extraction of nanocellulose fibrils from lignocellulosic fibres: A novel approach. *Carbohydr. Polym.* **2011**, *86*, 1468–1475. [[CrossRef](#)]
36. Staroń, P.; Chwastowski, J. Raphia-Microorganism Composite Biosorbent for Lead Ion Removal from Aqueous Solutions. *Materials* **2021**, *14*, 7482. [[CrossRef](#)] [[PubMed](#)]
37. Bassyouni, M.; Zoromba, M.S.; Abdel-Aziz, M.H.; Mosly, I. Extraction of Nanocellulose for Eco-Friendly Biocomposite Adsorbent for Wastewater Treatment. *Polymers* **2022**, *14*, 1852. [[CrossRef](#)]